ACS APPLIED ENERGY MATERIALS

www.acsaem.org Article

Microwave-Enabled Incorporation of Single Atomic Cu Catalytic Sites in Holey Graphene: Unifying Structural Requirements of a Carbon Matrix for Simultaneous Achievement of High Activity and Long-Term Durability

Qingdong Li, Hongbin Yang, Junjie Ouyang, Mikhail Solovyev, Nicole Lahanas, Carol Flach, Richard Mendelsohn, Eric Garfunkel, Michele Pavanello, Jenny V. Lockard,* and Huixin He*

Cite This: https://dx.doi.org/10.1021/acsaem.0c00704 Read Online

ACCESS | Metrics & More | Article Recommendations | Supporting Information

ABSTRACT: This work reports our discoveries from the first exploration in microwave pyrolysis of a metal−organic framework. A time- and energy-efficient approach was developed for direct fabrication of electrochemical single-atom catalysts (E-SACs) without the requirement of post-treatment. The most unique structure of the fabricated E-SAC is that the Cu catalytic sites were not in the amorphous carbon matrix as those achieved via traditional pyrolysis but in the basal planes of pristine holey graphene nanoplatelets. The as-prepared Cu-E-SAC exhibits excellent catalytic activity and selectivity in reducing oxygen to water in both acidic and alkaline media. The desired direct $4e^-$ pathway is more favorable in acidic versus alkaline media, which is different from all the Cu-E-SACs reported so far and most transition-metal-based E-SACs. The superior performance is attributed to the unique structure of the catalytic sites. The large graphene domains in the holey graphene materials provide higher delocalized electron-rich π band and increase the d-orbital energy level of the Cu centers. Consequently, their binding strength for molecular oxygen is largely enhanced, improving the oxygen reduction reaction and likely promoting a direct $4e^-$ pathway with minimized generation of a peroxide byproduct. Considering the high conductivity and excellent stability against oxidation of the holey graphene material, this work, for the first time, suggests that the contradictory structural requirement of a carbon matrix for high catalytic activity and long-term durability can be unified and simultaneously satisfied. Combined with the merits of simplicity and rapidness for fabricating both holey graphene and E-SACs, this work provides a possible strategy to address the critical challenges of precious metal-free single-atom catalysts.

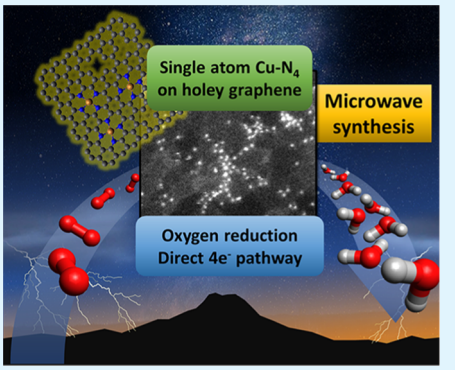

KEYWORDS: *ORR, single-atom catalysts, holey graphene, copper base catalyst, microwave synthesis*

1. INTRODUCTION

Single-atom catalysts (SACs) can simultaneously maximize the utilization of metal atoms and minimize side reactions, achieving high catalytic activity and selectivity, which are not attainable for the conventional nanoparticle-based catalysts.[1] SACs have been intensively investigated for a wide range of reactions and great progress has been achieved. The drive to replace precious platinum group metal (PGM)-based catalysts has led to a class of SACs of sustainable and inexpensive PGM-free electrocatalysts for the sluggish oxygen reduction reaction (ORR), in which the catalytic centers composed of transition metal ions are stabilized by nitrogen functional groups on carbonaceous surfaces ($M\text{-}N_xC_y$).[2,3] Despite recent great advances, numerous challenges still remain before PGM-free SACs become viable for large-scale practical application in proton-exchange membrane fuel cells (PEMFCs).[4] Currently, iron-based SACs (Fe-SACs) are the most promising and also most extensively studied PGM-free catalysts because of their encouraging ORR activity in acidic media.[5] However, even the state of the art of Fe-SACs could not satisfy the required catalytic efficiency and long-term durability for practical applications. There is a fundamental challenge for the carbon support to further improve these two critical performance parameters simultaneously.[6] Specifically, to further increase their catalytic efficiency, a highly disordered and defective carbon matrix is necessary to increase the density of accessible catalytic sites. It is also required to improve the activity of each Fe catalytic sites by downshifting the energy level of d-state of

Received: March 30, 2020
Accepted: August 4, 2020
Published: August 4, 2020

the Fe centers to weaken the adsorption of the ORR intermediates.[7,8] However, this defective carbon not only shows low conductivity but also shows low stability against oxidation. In the recent review articles, carbon matrix oxidation has been identified as the most important degradation mechanism of PGM-free catalysts in PEMFC cathodes.[9,10] The results of carbon matrix oxidation can cause catalyst flooding and demetalization of the active centers. The released Fe^{2+} ions in turn catalyze the decomposition of the possible byproduct of H_2O_2 and generate reactive oxidative species (ROS) via Fenton reaction.[11] Consequently, these ROS not only speed up the carbon matrix oxidation but also attack the components of PEMFCs such as ionomer and membrane, which is detrimental to the catalyst and fuel cell devices. On the other hand, defect-free graphene sheets are highly impervious against oxidative degradation, which is beneficial for long-term durability of a catalyst. They also provide high conductivity for assembling thick electrodes for practical applications.[9,10] However, it has been demonstrated that the carbon matrix with low defects not only largely decreased the density of the catalytic centers but also demoted the catalytic activity of each Fe center. The electron-rich π-band of the large defect-free graphene domains upshifts the energy level of the d-orbital of the Fe centers, further strengthening the absorption of the ORR intermediates.[7,8] The dilemma leads to insurmountable fundamental challenges in the development of Fe-based SACs that simultaneously satisfy the required high activity and durability for practical applications and call for actively pursuing non-Fe-based SACs.[11,12]

Another challenge for practical application of SACs is the lack of simple and economical methods to synthesize SACs with densely and uniformly dispersed accessible active sites.[13] Recently, metal−organic frameworks (MOFs) emerged as novel self-sacrificing precursors/templates to address these needs because of their built-in molecular level-controlled spatial arrangement of functional organic units, metallic sites, and porosity.[14−17] However, current procedures for converting MOFs to electrochemical single-atom catalysts (E-SACs) require a long- and high-temperature pyrolysis process under an inert or NH_3 environment. The time- and energy-consuming pyrolysis often leads to serious metal aggregation and/or formation of metal carbide and oxide nanoparticles, especially at high metal loadings to achieve high density of active sites. Even though some works reported that these metal particles might have played an auxiliary role to enhance the activity/selectivity of the electrocatalysts,[18,19] in most cases, their existence deteriorates the activity and selectivity of SACs. Furthermore, their formation decreases the density of the SAC sites and disturbs the study of origin of catalytic activities and selectivity to guide future development. A post-acid leaching treatment followed by an extra pyrolysis has been commonly applied to remove these metal nanoparticles without dramatic loss of the activity of the SAC centers.[20] Therefore, it is highly desirable to develop a facile method to convert the metal species in a designed MOF precursor to active SAC centers without metal aggregation.[21−23]

Here, we report the first exploration in microwave-assisted pyrolysis of a MOF to develop a time- and energy-efficient approach to fabricate E-SACs without metal aggregation. The initial hypothesis of this approach was based on the fast heating/cooling capability of microwave heating, which can quickly carbonize the organic linkers to a conductive carbon network, leaving no time for metal atoms to diffuse, so that all the designed metallic sites can be converted to single-atom catalytic sites.[13,24] Naturally, this synthetic approach avoids all the issues related to metal aggregation and the tedious post-treatment procedures associated with the formation of metal nanoparticles/aggregates.

As a demonstration, we began with the synthesis of Cu-E-SACs for electrocatalytic ORR using the copper porphyrin-based MOF, PCN-222-Cu. This MOF contains Zr-oxo cluster nodes connected by carboxyphenyl meso-substituted copper porphyrins to form a 3D porous architecture.[25] This MOF was chosen as the precursor following several considerations. First, theoretical calculations predicted that Cu possesses the uppermost activity for ORR among nonprecious transition metals because its position is the closest to Pt at the top of the "volcano plot."[26] Second, in nature, enzymes use Cu as the catalytic centers to reduce oxygen to water with 100% selectivity and low overpotential, which is even lower than Pt-based catalysts.[27,28] Furthermore, Cu-based catalysts do not promote the formation of hydroperoxyl and hydroxyl radical species (the so-called Fenton reagent), leading to enhanced durability during fuel cell operations.[29] Therefore, developing Cu-based SACs has the great potential to replace Pt with even lower operational overpotential and high durability compared to Fe-based SACs.[19] Despite these theoretical superiorities, Cu-based catalysts have shown much lower ORR activity compared to analogous Fe-based SACs as well as commercial Pt/C catalysts, leaving much to be improved for their practical application. However, the fabrication of Cu-based SAC is more challenging than that of Fe-based SACs because of the high diffusion constant of Cu at elevated fabrication temperatures.[19,30,31] Thus, to date, the study of Cu-based SACs has been much limited compared to Fe-based SACs,[29,32−34] especially in acidic conditions.[35−37] None of the Cu-based SACs reported so far have demonstrated higher selectivity toward a direct $4e^-$ process to water in acidic over alkaline media, which is currently desired catalysts for simple integration with the current PEM technologies.[35,38]

In this paper, we report that a Cu-E-SAC has been successfully fabricated with as short as 5 s of microwave irradiation in ambient conditions with no evidence of Cu atom aggregation. Unlike other reported MOF-derived E-SACs prepared by traditional pyrolysis, the Cu-active centers were incorporated in the holey graphene (hG) nanoplatelets, as evidenced by high-resolution high-angle annular dark-field scanning transmission electron microscopy (HAADF−STEM) and electron energy loss spectroscopy (EELS). Considering the large defect-free graphene domains in the hG nanoplatelets, we surprisingly found that the as-prepared Cu-SAC exhibits much improved (not decreased as in the case of Fe-SACs[7,8]) catalytic activity and selectivity in reducing molecular oxygen to water. The selectivity via the desired direct $4e^-$ pathway in acidic media is even higher than that in alkaline media, which is different from all the Cu-E-SACs reported so far.[2,35,39,40] Given the high conductivity and excellent stability against oxidation of the hG material, this work, for the first time, suggests that the contradictory structural requirement of a carbon matrix for high catalytic activity and long-term durability can be unified and simultaneously satisfied.

2. RESULTS AND DISCUSSION

2.1. Microwave Pyrolysis of MOF. Although microwave heating is often used to facilitate organic reactions and to fabricate various nanomaterials,[41,42] including MOF particles,[43]

https://dx.doi.org/10.1021/acsaem.0c00704
ACS Appl. Energy Mater. XXXX, XXX, XXX−XXX

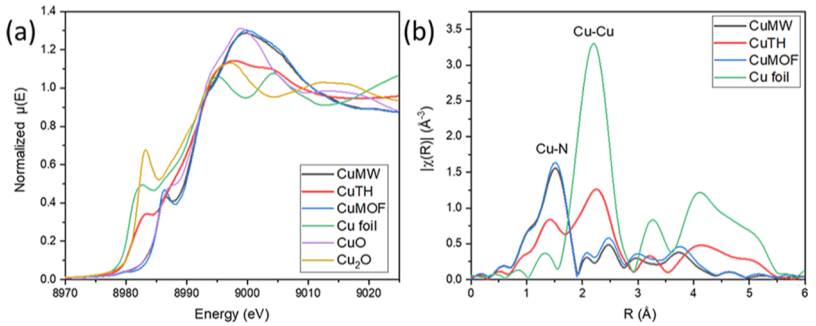

Figure 1. Cu K-edge (a) XANES and (b) EXAFS spectra of CuMW, CuTH, CuMOF, and Cu foil and oxide references.

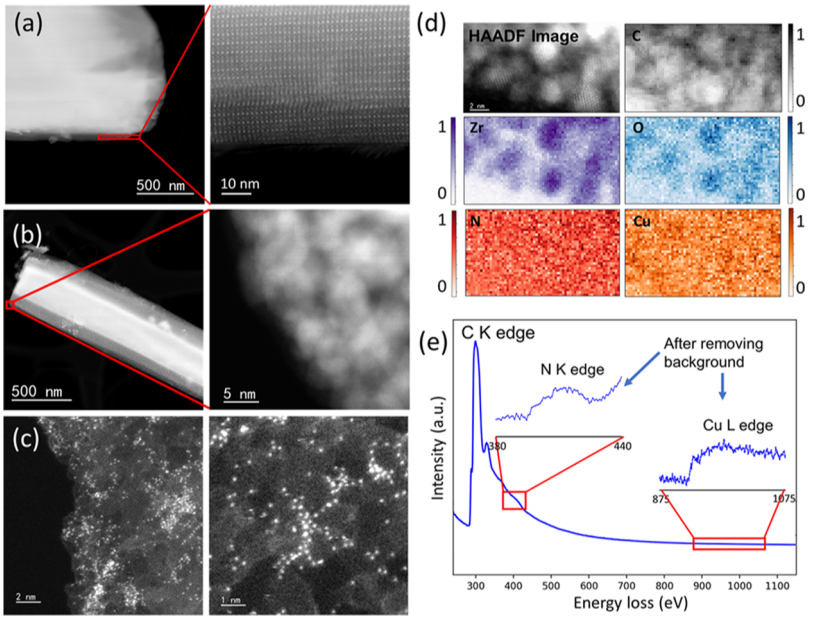

Figure 2. HAADF images of CuMOF before (a) and after (b) microwave irradiation. (c) hG part of CuMW and (d) EELS mapping of the MOF part in CuMW. (e) EELS averaged from an 8 × 8 nm^2 on the hG part of CuMW.

it has never been used for pyrolysis of an MOF for E-SAC fabrication. Most MOFs are microwave transparent and therefore cannot be directly pyrolyzed via microwave heating. Addition of microwave absorbers to the reaction system enables microwave-assisted reactions, especially in solvent-free conditions.[44,45] Our key concept for the conversion of an MOF to an E-SAC builds on the ability to abruptly raise and decrease the temperature in a large range, so that the organic linkers carbonize rapidly at high temperature, confining the movement of the metal atoms, and then cool down instantly, leaving no time for their diffusion and aggregation. Multilayer graphene due to its high electron conductivity is able to efficiently convert microwave energy to heat, quickly generating high temperature in seconds.[46,47] To guarantee high electron conductivity of the microwave absorbing carbon, a very small amount of carbon nanotube is mixed with hG nanoplatelets.[48] With a short microwave irradiation, a high-temperature thermal shock is generated, evidenced by the bright white arcing.[46,47] The microwave power and duration were optimized to 300 W and 5 s (Figures S5−S7), and the resulting sample is named as CuMW. As a control, we also applied the traditional pyrolysis method to fabricate Cu-based electrocatalysts from PCN-222-Cu using three selected temperatures, 700, 1000, and 1100 °C. The resulting catalysts were named as CuTH, Cu-TH-1000, and Cu-TH-1100, respectively. CuTH was acid-leached, leaving only the single-atom Cu in the catalyst. This sample was denoted as CuTHa.

2.2. X-ray Absorption Spectroscopy. We first characterized the as-prepared electrocatalysts by Cu K-edge X-ray absorption spectroscopy (XAS), which provides element-specific electronic and local structural information about the Cu sites within these materials. Figure 1 shows both X-ray near-edge spectroscopy (XANES) and extended X-ray absorption fine structure (EXAFS) data for the samples achieved via microwave heating. Comparison with several reference systems, including metallic Cu, copper oxides, and the PCN-222-Cu precursor, suggests that upon MW treatment, the Cu sites maintained similar speciation to that in the porphyritic structures of the parent MOF material. The XANES edge energy indicates a Cu^{2+} oxidation state, and the 1s → 4p "shakedown" feature at 8986.3 eV indicates that the square-planar structure of $Cu-N_4$ in the Cu−porphyrin is largely preserved.[49,50] The EXAFS spectra of the CuMW sample lack the characteristic Cu−Cu peak observed for metallic species, demonstrating that microwave heating can effectively avoid metal aggregation and all the Cu atoms remain in the isolated form (Figure 1). Although XAS characterization suggests that some Cu−porphyrin was destroyed upon increased microwave irradiation time (Figure S2), there was still no evidence for Cu aggregation.

https://dx.doi.org/10.1021/acsaem.0c00704
ACS Appl. Energy Mater. XXXX, XXX, XXX−XXX

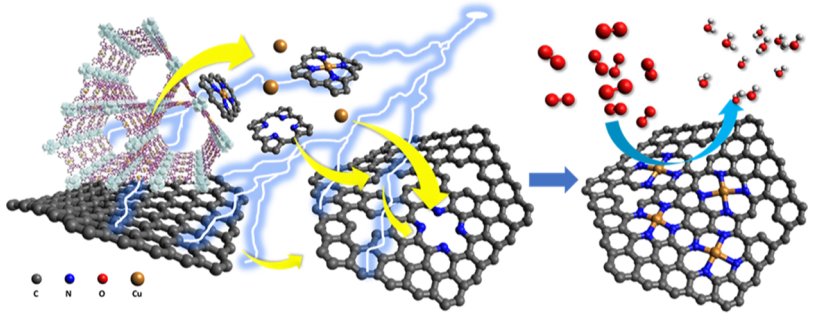

Figure 3. Microwave synthesis of Cu-E-SACs. Under microwave irradiation, carbon vacancies are generated on nearly pristine basal planes of hG, leaving other parts of the graphene sheets nearly intact. In the same time, some Cu−porphyrin species, either as a Cu−porphyrin complex or separated Cu and porphyrin species, emitted out from the MOF with the high temperature generated by the microwave heating. These emitted species subsequently doped into the in situ generated vacancies forming the singe Cu atom catalytic sites.

In high contrast, the porphyritic structures were largely destroyed in the samples produced via traditional heating as evident in Figure 1, with complete destruction evident at the most elevated temperatures up to 1100 °C. The XANES spectra for CuTH reveal an edge shift, indicating a large presence of Cu^0 species, and the EXAFS spectra clearly contain a Cu−Cu scattering peak. The XAS spectra, shown in Figure S3, provide strong evidence for substantial metal aggregation, even at the milder pyrolysis at 700 °C. Note that this temperature was 100 °C lower than that used for PCN-222-Fe by Jiang et al.,[22] in accordance with the fact that Cu is more diffusive than Fe.[19,30,31] The EXAFS spectra of the acid-leaching treated sample CuTHa possesses no Cu−Cu peak (Figure S4), proving successful removal of Cu aggregates.

2.3. STEM-EELS Characterization. To further confirm the single-atom dispersion and the uniformity of catalytic sites, STEM and EELS were applied to study the microwave-pyrolyzed samples. Compared to the XAS techniques, STEM and EELS offer high spatial resolution that allow us to study the change of both the MOF particles and the carbon nanomaterials upon microwave irradiation. Figure 2a shows an HAADF image of a typical MOF crystal before pyrolysis. The periodically arranged high-intensity white dots are possibly Zr-oxo node clusters. The low atomic mass of Cu (29) compared with that of Zr (40) makes it difficult to identify the Cu atoms during HAADF imaging even if they are present. Upon a short microwave pyrolysis, the original periodical arrangement of these clusters transformed into densely packed nanoparticles of 2−3 nm (Figure 2b). Core loss EELS mapping clearly demonstrated that these nanoparticles are zirconium oxide, which are dispersed in the carbon matrix derived from the organic part of the MOF crystal (Figure 2d). A negligible amount of nitrogen and copper was detected in the mapped area of the pyrolyzed MOF, indicating that neither copper aggregates nor oxides were formed after microwave irradiation because the detection of aggregated Cu particles is relatively easy compared to single Cu atoms. To our surprise, we found a lot of single dispersed metal atoms located on hG sheets, as shown in Figure 2c. These single dispersed metal atoms are identified to be Cu, which are coordinated with N with a Cu-to-N ratio of around 1:4 by EELS (Figure 2e). These results suggest that hG was not only acting as the microwave absorber but also as the substrate into which the single metal atoms incorporated.

It is widely accepted when an MOF is used as a self-templating precursor, the metal components, either in the form of coordinates with N or metal nanoparticles (metal, carbide, or nitride), all located on or embedded in the newly formed carbon surfaces from graphitization of the organic linkers.[14−17] Both HAADF−STEM and EELS results unambiguously suggested that microwave-assisted pyrolysis indeed led to rapid formation of SAC as expected. However, the observation of relocation of the Cu single atoms to the hG planes was out of our predication. We originally hypothesized that the high temperature achieved via microwave heating could facilitate carbonization of the organic linkers and activation of the Cu porphyrin units to Cu-SAC centers. At the same time, the rapid quenching possibly impedes migration/diffusion of Cu atoms, thereby ensuring the uniform dispersion of Cu-SAC centers embedded in a conductive carbon matrix without aggregation. Rather than preventing metal atom diffusion however, microwave heating instead appears to have accelerated it, resulting in Cu atoms flying out the surface of the MOF particles to hG to form the Cu single-atom sites. EELS demonstrated that these Cu atoms are possibly coordinated with four nitrogen atoms (Figure 2e), similar to the structure of the Cu−porphyrin in the MOF determined by the XANES study (Figure 1).

At present, the formation mechanism of the active sites is not clear and worth further studies. In our previous study, we found that microwave irradiation of defect-free graphene flakes could lead to generation of nanoholes in the basal planes of graphene, leaving other parts of the basal plane nearly intact.[51] In the present study, with the high-resolution HAADF−STEM imaging, we found that under microwave irradiation, carbon vacancies are generated on the basal planes of hG. We hypothesize that with the high temperature generated by microwave heating, some Cu−porphyrin species, either as a Cu−porphyrin complex, or separated Cu and porphyrin species, emitted out from the MOF.[35,52] These emitted species subsequently doped into the in situ-generated vacancies forming the singe Cu atom sites, which are likely to be the electrocatalytically active centers for ORR (Figure 3).

On the other hand, after microwave irradiation, a composite shell is formed on the MOF particles, mainly composited of zirconium oxide nanoparticles and amorphous carbon. Some $Cu-N_4$ species were also possibly incorporated in this shell (Figure 2b,d). Most of the Cu−porphyrin remains intact inside the MOF as evidenced from the XAS studies. These Cu−porphyrin structures are likely remaining inactive to ORR as those in the original PCN-222-Cu MOF. The Cu species incorporated in the composite shell might not be ORR active either based on the following consideration: the graphitization level of the organic linkers in the MOF is very low, as indicated

https://dx.doi.org/10.1021/acsaem.0c00704
ACS Appl. Energy Mater. XXXX, XXX, XXX−XXX

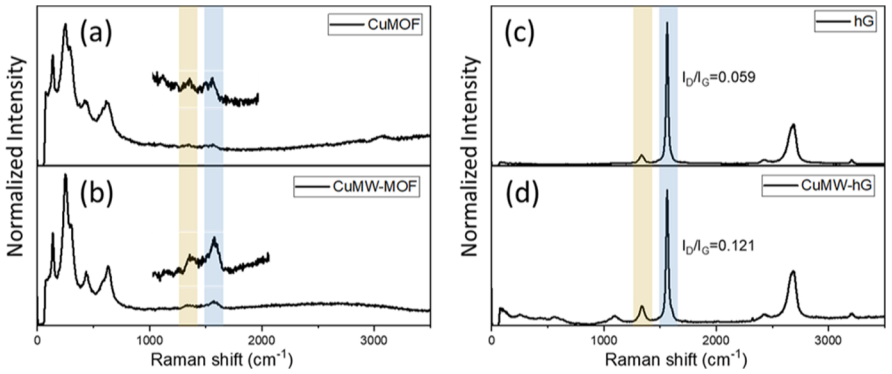

Figure 4. Raman spectroscopy of (a) CuMOF, (b) MOF part of the CuMW, (c) hG, and (d) hG part of the CuMW.

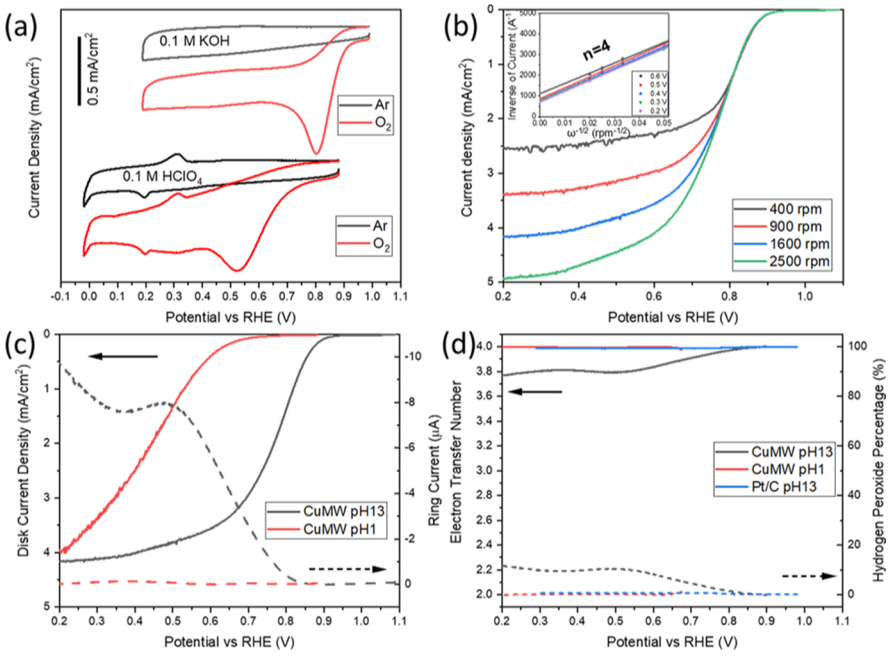

Figure 5. (a) CV of CuMW in both Ar-saturated and O_2-saturated 0.1 M KOH and 0.1 M $HClO_4$ at a scan rate of 10 mV/s. (b) LSV of CuMW in 0.1 M KOH at 10 mV/s with various rotation speeds. The inset shows the corresponding K–L plot. (c) LSV of CuMW showing disk current density (solid line) and ring current (dashed line) in O_2-saturated 0.1 M KOH and 0.1 M $HClO_4$ at a scan rate of 10 mV/s. (d) Electron-transfer number (solid line) and hydrogen peroxide percentage (dashed line) of CuMW and Pt/C in O_2-saturated 0.1 M KOH and 0.1 M $HClO_4$ calculated using the RRDE method.

by the similar low intensity and less defined peak shapes of the G and D bands in the Raman spectra of MOF particles before and after microwave irradiation (Figure 4a,b). Combined with the insulator nature of zirconium oxide nanoparticles, the composite shell is likely nonconductive; therefore, the Cu species incorporated in the composite shell are not electronically connected to be ORR active. In high contrast, the G band of hG remains well defined with high intensity, and the intensity ratio of D to G bands just slightly increased from 0.059 to 0.121(Figure 4c,d), possibly arising from the incorporation of $Cu-N_4$ into their basal planes. The low D/G band ratio suggests that hG, where the $Cu-N_4$ sites are incorporated, has much larger defect-free graphene domains.[53] This feature is very different from the previously reported PGM-free SACs, including Fe-, Cr-, Mn-, and Cu-based SACs.[4,7,11,22,35,54,55] These $Cu-N_4$ sites on hG are not only easily accessible but also the electron-transfer rate on the graphene is much faster than those on/in amorphous carbon in general.[56]

2.4. Electrochemical Studies. The catalytic activity of the microwave-pyrolyzed catalyst (CuMW) was evaluated with multiple electrochemical techniques. First, cyclic voltammetry (CV) was performed in both Ar- and O_2-saturated 0.1 KOH solutions. A large reduction peak was observed in the O_2-saturated electrolytes. However, this peak was absent in the Ar-saturated solutions, suggesting that the CuMW catalyst is active in catalyzing molecular oxygen reduction (Figure 5a). The onset (E_{onset} = 0.92 V *vs* RHE), half wave ($E_{1/2}$ = 0.86 V), and peak potential (E_p = 0.8 V) are among the top performing Cu-based catalysts reported in basic media as shown in the Supporting Information, Table S2. A control experiment has been performed to pyrolyze a PCN-222 MOF in which there was no Cu centers in its porphyrin structures. The resulting material exhibited low ORR performance as the carbon nanomaterial alone without an MOF (Figure S8), demonstrating the essential role of Cu centers in CuMW to the observed high catalytic activity. Linear sweep voltammetry (LSV) with a rotating ring disk electrode (RRDE) was used to study the

https://dx.doi.org/10.1021/acsaem.0c00704
ACS Appl. Energy Mater. XXXX, XXX, XXX–XXX

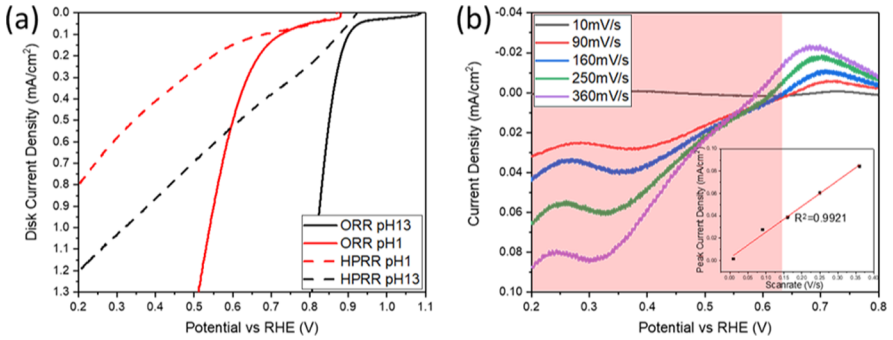

Figure 6. (a) LSV of ORR (solid line) and HPRR (dash line) catalyzed by CuMW in both acidic and basic media. (b) Differential CV in Ar-saturated 0.1 M $HClO_4$ for CuMW. The red region shows the reduction of the absorbed O_2 on the CuN_4-active site. The inset shows the linear relationship between the peak current density and scan rate for the red region of CuMW.

kinetics and mechanism of ORR. The apparent electron-transfer number at 0.5 V (*vs* RHE) calculated from the K–L plot was ~4 (Figure 5b). The catalyst also exhibits excellent tolerance to methanol (Supporting Information, Figure S10). In comparison, the catalyst (CuTHa) achieved via traditional heating of a PCN-222-Cu MOF showed much lower kinetic current density (Supporting Information, Figures S11 and S12). Its onset potential was also largely negatively shifted (0.85 V *vs* RHE). After an acid treatment, the Cu aggregates were removed, and the resulting CuTHa has similar $Cu-N_4$ structures to that of CuMW, demonstrated by the X-ray fine structure spectroscopy studies (Figure S4). Even though, the current density of CuTHa was increased slightly compared to CuTH, but still much lower than that of CuMW. Furthermore, the apparent electron-transfer number of CuTHa was also much lower (~2.9 to 3.4). All these results demonstrated that the microwave-enabled approach is not only simple and fast, and the fabricated Cu-E-SAC also exhibits much improved catalytic activity compared to that achieved via traditional heating approach.

Encouraged by the appealing performance described above, we carefully studied the catalytic behavior of CuMW in acidic media, which is more attractive for easily dropping into the current fuel cell applications. The onset potential is negatively shifted (E_{onset} = 0.8 V), and the geometric kinetic current density is lower than that in an alkaline solution (Figure 5c). No observable diffusion-limited region was identified in 0.1 M $HClO_4$, indicating kinetic control even at high overpotentials. The lower catalytic activity in an acidic solution compared to that in an alkaline solution is very similar to that of other SACs, such as Fe and Mn,[11] Cr,[12] and Cu-SACs prepared by a thermal emitting method reported by Li et al.,[35] which has been attributed to the lower activity of the catalytic centers in acidic than in alkaline environments in general. However, to our delighted surprise, the apparent electron-transfer number (n) is also 4.0 at 0.5 V (*vs* RHE).

In general, the measured apparent $4e^-$ pathway during electroreduction of oxygen maybe through a direct $4e^-$ pathway ($O_2 \rightarrow H_2O$) or via indirect pathways involving a H_2O_2 intermediate in acidic conditions or HO_2^- in basic electrolytes.[8,57,58] By rotating the RRDE electrode, H_2O_2 (or HO_2^- in basic media) intermediates, if generated and desorbed from the catalytic surface on the disk electrode, can be quickly spread onto the ring electrode and immediately get oxidized on the ring electrode where a constant high voltage is applied. Thus, the ring current is an indication of H_2O_2 (or HO_2^-) generation and desorption from the catalyst surface. It has been reported that the interaction of H_2O_2 with single atom-based catalytic centers is much weaker than that of HO_2^-, so if H_2O_2 intermediates were generated during ORR, they have stronger tendency to be desorbed from the catalytic center to the bulk electrolyte and being detected at the ring electrode in acidic media.[8,57,58] This is one of the important reasons that all the transition-metal-based E-SACs exhibit higher $4e^-$ selectivity in basic media compared to that in acid media. It is very interesting to observe that the ring current due to peroxide oxidation in acidic condition is much lower (15 times lower at ~0.5 V) than that measured in alkaline solutions (Figure 5c). Furthermore, even though the disk current due to ORR largely increases as the potential becomes more negative, the ring current remains low in the entire potential region and does not show any significant increase in the scanned potential range. The apparent electron-transfer number (n) calculated from RRDE results is 4.0 in the entire scanned potential window, similar to that observed on the Pt/C catalyst (Figure 5d). This is in high contrast to that observed in alkaline solutions. The apparent electron-transfer number (n) decreased from 4.0 to 3.8 as the overpotential increases. These results clearly suggest that CuMW has higher selectivity toward water via the desired $4e^-$ pathway in acidic than that in alkaline solutions, which are different from all the Cu-E-SACs reported so far and most transition-metal-based E-SACs.

The extremely low current measured on the ring electrode suggests that there was either no H_2O_2 intermediates generated on the CuMW catalytic surface in acidic media or they were rapidly reduced to water because of the strong bonding strength and catalytic activity of the active centers to H_2O_2.[8,57,58] This pathway has been commonly referred as an indirect (sequential $2e^- \times 2e^-$) pathway during ORR. To further understand whether the ORR experienced an indirect (sequential $2e^- \times 2e^-$) or direct $4e^-$ pathway, hydrogen peroxide reduction reaction (HPRR) was performed under the same conditions as those for ORR except the electrolytes were Ar-saturated (oxygen free) and containing 2 mM hydrogen peroxide. As shown in Figure 6a, the HPRR is kinetically much slower than ORR in both alkaline and acidic media. The current density for HPRR in acidic media is even lower than that in alkaline media.

All the results described above merged and suggested that the Cu-active site in CuMW shows weaker interaction with H_2O_2 and also lower catalytic activity to reduce H_2O_2 to water. The high activity and selectivity for direct reduction of molecular oxygen to water is likely due to the strong interaction between the catalytic sites with molecular oxygen.

https://dx.doi.org/10.1021/acsaem.0c00704
ACS Appl. Energy Mater. XXXX, XXX, XXX–XXX

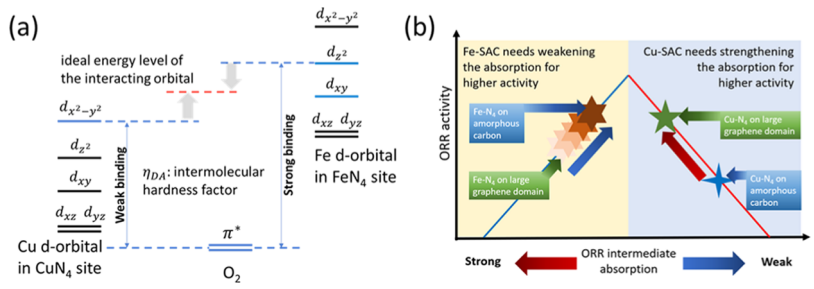

Figure 7. (a) Relationship between intermolecular hardness and bond strength (blue bars: energy levels of orbitals that are involved in the bond between the active site and the adsorbate). (b) Position of the CuN_4 site in a volcano plot for ORR based on the Sabatier principle.

To experimentally demonstrate this hypothesis, we designed the following experiment to study the oxygen absorption capability of the CuMW catalyst. The experimental protocol was designed according to the report by Specchia et al.[2] with some modifications to remove the influence of decreased oxygen concentration in the electrolyte after the first CV cycle. Specifically, CV was performed first in argon-saturated 0.1 M $HClO_4$ at various scan rates (CV-Ar). Then, the electrode was soaked in O_2-saturated electrolyte for 5 min with rotation to allow absorption of oxygen onto the catalyst surface. Subsequently, CV was performed again in oxygen-free (Ar-saturated) solution, which is denoted as CV-O_2. The soaking and subsequent CV processes were repeated with different scan rates. Subtraction of CV-Ar from CV-O_2 gives the reduction current of the absorbed O_2, eliminating the reduction of O_2 diffused from the bulk solution and the charging current. As shown in Figure 6b, a peak shows up at 0.55−0.3 V, which is assigned as oxygen reduction. Its peak current density (I_p) varies linearly with the scan rate ν (instead of the square root of the scan rate, $\nu^{1/2}$), which is a characteristic of surface-bound species, further confirming that the measured ORR current is indeed from oxygen molecules which have already absorbed on the catalytic surface.[59] O_2 absorption on the Cu-SAC fabricated with traditional heating (CuTHa) was also studied using the same method. Even though oxygen reduction current also showed up in the differential CVs (Figure S13), the current density is significantly low, indicating the weak O_2 absorption capability of CuTHa, which is consistent with other reported Cu-SACs and Cu macrocycle molecules.[39,40] The much higher peak current density in CuMW compared to that of CuTHa clearly demonstrated that the catalytic surface of Cu-SAC fabricated via microwave heating has much stronger interaction with molecular oxygen than that achieved via the traditional heating approach.

It has been widely accepted that the electrocatalytic activity and selectivity of M-SAC depends on the energy level and electron density of the d-orbital of the metal centers, which are different depending on the metal centers and their coordination environments (MN_xC_y, M = Fe, Co, Mn, Cu, etc.).[7,40] The interaction of the catalytic sites with the carbonaceous substrates also plays a key role in tuning the charge density and the d-orbital states of the metal-active sites, enabling optimization of the adsorption energy for the intermediates on the catalytic sites.[6−8] Higher energy level of the d-orbital in the M−N_4 sites induces a large intermolecular hardness factor (η_{DA}) of the bond between M−N_4 catalytic sites and molecular oxygen/ORR intermediates, resulting in their strong adsorption on the catalytic centers. We hypothesized that the nearly defect-free hG structural feature in Cu-MW provides highly delocalized π electrons to increase the electron density and upshift the energy level of the d-orbital Cu catalytic site, which results in much enhanced bond strength with molecular oxygen (Figure 7). This hypothesis is further supported with density functional theory (DFT) calculations (Supporting Information, Section S8 and Figure S14). The strengthened interaction in turn improves the catalytic activity and selectivity of direct 4e$^-$ pathway, yielding less H_2O_2 byproduct.

It is noteworthy that this is an opposite scenario to the case of Fe-based SACs. It is widely accepted that the activity of Fe-active centers is limited by the strong chemisorption bond strength of the ORR intermediates. Ramaswamy et al. demonstrated that highly disordered carbon substrates with stronger electron-withdrawing capability were required to weaken the absorption energy by downshifting the energy level of the d-orbital of the Fe center, thus enhancing the catalytic activity of the Fe-active centers.[8] While considering the low stability of the highly disordered carbon substrates, it has been an insurmountable fundamental challenge in the development of Fe-based SACs to simultaneously satisfy the requirement to further improve both high activity and durability for practical applications. In high contrast, the nearly defect-free hG support is not only highly conductive but is also highly resistant against oxidation.[48] Combined with the high activity and selectivity of CuMW catalysts in the reduction of oxygen directly to water with minimal generation of H_2O_2 byproduct, this work suggested that the opposite structural requirement of a carbon matrix to simultaneously improve the catalytic activity and stability against oxidation can be simultaneously satisfied.

3. CONCLUSIONS

In summary, the microwave heating approach reported in this work enables fast fabrication of Cu-based electrochemical single atomic catalysts (Cu-E-SAC) without the formation of metal aggregates. Accordingly, all the metal aggregate-related and post-treatment issues are naturally avoided. Most importantly, the catalytic centers are incorporated in hG nanoplatelets instead of a highly defective amorphous carbon matrix as most reported E-SACs. The as-prepared Cu-E-SAC exhibits excellent ORR performance in catalytic activity and selectivity in the reduction of molecular oxygen to water in both acidic and alkaline media. It is especially interesting that the selectivity of this catalyst reported here to water via the desired direct 4e$^-$ pathway is even more favorable in acidic media than that in alkaline media. Combining the non/low activity of Cu ions to active H_2O_2 in generating SOC, the issues related to SOC oxidation of ionomers, membranes, and carbon matrix should be largely avoided, promoting a more

https://dx.doi.org/10.1021/acsaem.0c00704
ACS Appl. Energy Mater. XXXX, XXX, XXX−XXX

durable catalyst.[9] Furthermore, this work demonstrated that incorporating Cu-SAC in highly graphitized graphene sheets could improve the activity of Cu-SAC over an amorphous carbon matrix, which is contrast to the widely studied Fe-based SACs.[6−8] For the first time, it is demonstrated that the opposite structural requirements for the carbon matrix in improving the catalytic activity and durability are unified. Furthermore, hG instead of defect-free graphene as the carbon matrix has the following further advantages: (1) the existence of a large of amount of different sizes of holes from micrometer to nanometer increased the mass transport[13,60,61] and (2) the nearly defect-free feature on their basal planes increases the hydrophobicity (against flooding)/high conductivity (better for thick practical electrodes).[5,6,9] All these combined with the merits of simplicity and rapidness for fabricating both hG materials and E-SACs, this work provides another possible strategy to tackle some of the critical challenges of precious metal-free single-atom catalysts. Although the onset potential of this catalyst is still lower than that of Pt and Fe-SACs, further tuning the electronic structure of the Cu-active centers, such as introduction of electron-donating heteroatoms in the carbon support and/or designing dinuclear metallic catalytic centers, will possibly solve these problems. Furthermore, considering the unique formation mechanism of the catalytic centers, it is reasonable to assume that the expensive porphyrin-based MOF precursor can be replaced with cheap metal salts and N-containing compounds to further reduce the product cost, which are currently under study in our lab.

■ ASSOCIATED CONTENT

Supporting Information

The Supporting Information is available free of charge at https://pubs.acs.org/doi/10.1021/acsaem.0c00704.

Detailed DFT calculation, experimental procedures, and optimization of the fabrication and characterization of the catalysts (PDF)

■ AUTHOR INFORMATION

Corresponding Authors

Jenny V. Lockard − *Department of Chemistry, Rutgers, The State University of New Jersey, Newark, New Jersey 07102, United States*; Email: jlockard@newark.rutgers.edu

Huixin He − *Department of Chemistry, Rutgers, The State University of New Jersey, Newark, New Jersey 07102, United States*; Email: huixinhe@newark.rutgers.edu

Authors

Qingdong Li − *Department of Chemistry, Rutgers, The State University of New Jersey, Newark, New Jersey 07102, United States*; orcid.org/0000-0003-4089-7425

Hongbin Yang − *Department of Chemistry and Chemical Biology, Rutgers University, New Brunswick, New Jersey 08901, United States*; orcid.org/0000-0002-0098-6944

Junjie Ouyang − *Department of Chemistry, Rutgers, The State University of New Jersey, Newark, New Jersey 07102, United States*

Mikhail Solovyev − *Department of Chemistry, Rutgers, The State University of New Jersey, Newark, New Jersey 07102, United States*

Nicole Lahanas − *Department of Chemistry, Rutgers, The State University of New Jersey, Newark, New Jersey 07102, United States*

Carol Flach − *Department of Chemistry, Rutgers, The State University of New Jersey, Newark, New Jersey 07102, United States*

Richard Mendelsohn − *Department of Chemistry, Rutgers, The State University of New Jersey, Newark, New Jersey 07102, United States*

Eric Garfunkel − *Department of Chemistry and Chemical Biology, Rutgers University, New Brunswick, New Jersey 08901, United States*

Michele Pavanello − *Department of Chemistry, Rutgers, The State University of New Jersey, Newark, New Jersey 07102, United States*; orcid.org/0000-0001-8294-7481

Complete contact information is available at: https://pubs.acs.org/10.1021/acsaem.0c00704

Notes

The authors declare no competing financial interest.

■ ACKNOWLEDGMENTS

H.H. and M.P. would acknowledge the support by the National Science Foundation under grant DMR-1742807. H.H. would also acknowledge the support by the ACS Petroleum Research Fund under grant 58557-ND5. J.V.L. would like to acknowledge the support by the National Science Foundation under grant no. DMR-1455127. Part of this work is based on the research conducted at the Advanced Photon Source (APS), an Office of Science User Facility operated for the U.S. Department of Energy (DOE) Office of Science by Argonne National Laboratory and was supported by the U.S. DOE under contract no. DE-AC02-06CH11357. Part of this research used beamline 6BM of the National Synchrotron Light Source II, a U.S. Department of Energy (DOE) Office of Science User Facility operated for the DOE Office of Science by Brookhaven National Laboratory under contract no. DE-SC0012704. M.S. was supported by a U.S. Department of Energy (DOE) Office of Science Graduate Student Research (SCGSR) award. We thank Dr. Chengjun Sun for support during XAS measurements at APS and Dr. Bruce Ravel for support during XAS measurements at NSLS II.

■ REFERENCES

(1) Yang, X.-F.; Wang, A.; Qiao, B.; Li, J.; Liu, J.; Zhang, T. Single-Atom Catalysts: A New Frontier in Heterogeneous Catalysis. *Acc. Chem. Res.* **2013**, *46*, 1740−1748.

(2) Osmieri, L.; Monteverde Videla, A. H. A.; Ocón, P.; Specchia, S. Kinetics of Oxygen Electroreduction on Me-N-C (Me = Fe, Co, Cu) Catalysts in Acidic Medium: Insights on the Effect of the Transition Metal. *J. Phys. Chem. C* **2017**, *121*, 17796−17817.

(3) Zagal, J. H.; Koper, M. T. M. Reactivity Descriptors for the Activity of Molecular MN4 Catalysts for the Oxygen Reduction Reaction. *Angew. Chem., Int. Ed.* **2016**, *55*, 14510−14521.

(4) Wan, X.; Liu, X.; Li, Y.; Yu, R.; Zheng, L.; Yan, W.; Wang, H.; Xu, M.; Shui, J. Fe-N-C electrocatalyst with dense active sites and efficient mass transport for high-performance proton exchange membrane fuel cells. *Nat. Catal.* **2019**, *2*, 259−268.

(5) Martinez, U.; Babu, S. K.; Holby, E. F.; Chung, H. T.; Yin, X.; Zelenay, P. Progress in the Development of Fe-Based PGM-Free Electrocatalysts for the Oxygen Reduction Reaction. *Adv. Mater.* **2019**, *31*, 1970224.

(6) Asset, T.; Atanassov, P. Iron-Nitrogen-Carbon Catalysts for Proton Exchange Membrane Fuel Cells. *Joule* **2020**, *4*, 33−44.

(7) Mun, Y.; Lee, S.; Kim, K.; Kim, S.; Lee, S.; Han, J. W.; Lee, J. Versatile Strategy for Tuning ORR Activity of a Single Fe-N4 Site by

Controlling Electron-Withdrawing/Donating Properties of a Carbon Plane. *J. Am. Chem. Soc.* **2019**, *141*, 6254−6262.
(8) Ramaswamy, N.; Tylus, U.; Jia, Q.; Mukerjee, S. Activity Descriptor Identification for Oxygen Reduction on Nonprecious Electrocatalysts: Linking Surface Science to Coordination Chemistry. *J. Am. Chem. Soc.* **2013**, *135*, 15443−15449.
(9) Shao, Y.; Dodelet, J. P.; Wu, G.; Zelenay, P. PGM-Free Cathode Catalysts for PEM Fuel Cells: A Mini-Review on Stability Challenges. *Adv. Mater.* **2019**, *31*, 1807615.
(10) Tian, X.; Lu, X. F.; Xia, B. Y.; Lou, X. W. Advanced Electrocatalysts for the Oxygen Reduction Reaction in Energy Conversion Technologies. *Joule* **2020**, *4*, 45−68.
(11) Li, J.; Chen, M.; Cullen, D. A.; Hwang, S.; Wang, M.; Li, B.; Liu, K.; Karakalos, S.; Lucero, M.; Zhang, H.; Lei, C.; Xu, H.; Sterbinsky, G. E.; Feng, Z.; Su, D.; More, K. L.; Wang, G.; Wang, Z.; Wu, G. Atomically dispersed manganese catalysts for oxygen reduction in proton-exchange membrane fuel cells. *Nat. Catal.* **2018**, *1*, 935−945.
(12) Luo, E.; Zhang, H.; Wang, X.; Gao, L.; Gong, L.; Zhao, T.; Jin, Z.; Ge, J.; Jiang, Z.; Liu, C.; Xing, W. Single-Atom Cr-N4 Sites Designed for Durable Oxygen Reduction Catalysis in Acid Media. *Angew. Chem., Int. Ed.* **2019**, *58*, 12469.
(13) Fei, H.; Dong, J.; Wan, C.; Zhao, Z.; Xu, X.; Lin, Z.; Wang, Y.; Liu, H.; Zang, K.; Luo, J.; Zhao, S.; Hu, W.; Yan, W.; Shakir, I.; Huang, Y.; Duan, X. Microwave-Assisted Rapid Synthesis of Graphene-Supported Single Atomic Metals. *Adv. Mater.* **2018**, *30*, 1802146.
(14) Li, L.; He, J.; Wang, Y.; Lv, X.; Gu, X.; Dai, P.; Liu, D.; Zhao, X. Metal-organic frameworks: a promising platform for constructing non-noble electrocatalysts for the oxygen-reduction reaction. *J. Mater. Chem. A* **2019**, *7*, 1964−1988.
(15) Zhang, H.; Liu, X.; Wu, Y.; Guan, C.; Cheetham, A. K.; Wang, J. MOF-derived nanohybrids for electrocatalysis and energy storage: current status and perspectives. *Chem. Commun.* **2018**, *54*, 5268−5288.
(16) Liu, J.; Zhu, D.; Guo, C.; Vasileff, A.; Qiao, S.-Z. Design Strategies toward Advanced MOF-Derived Electrocatalysts for Energy-Conversion Reactions. *Adv. Energy Mater.* **2017**, *7*, 1700518.
(17) Barkholtz, H. M.; Liu, D.-J. Advancements in rationally designed PGM-free fuel cell catalysts derived from metal-organic frameworks. *Mater. Horiz.* **2017**, *4*, 20−37.
(18) Jiang, W.-J.; Gu, L.; Li, L.; Zhang, Y.; Zhang, X.; Zhang, L.-J.; Wang, J.-Q.; Hu, J.-S.; Wei, Z.; Wan, L.-J. Understanding the High Activity of Fe-N-C Electrocatalysts in Oxygen Reduction: Fe/Fe3C Nanoparticles Boost the Activity of Fe-Nx. *J. Am. Chem. Soc.* **2016**, *138*, 3570−3578.
(19) Wang, J.; Wang, K.; Wang, F.-B.; Xia, X.-H. Bioinspired copper catalyst effective for both reduction and evolution of oxygen. *Nat. Commun.* **2014**, *5*, 5285.
(20) Herranz, J.; Jaouen, F.; Lefèvre, M.; Kramm, U. I.; Proietti, E.; Dodelet, J.-P.; Bogdanoff, P.; Fiechter, S.; Abs-Wurmbach, I.; Bertrand, P.; Arruda, T. M.; Mukerjee, S. Unveiling N-Protonation and Anion-Binding Effects on Fe/N/C Catalysts for O-2 Reduction in Proton-Exchange-Membrane Fuel Cells. *J. Phys. Chem. C* **2011**, *115*, 16087−16097.
(21) Zhang, H.; Hwang, S.; Wang, M.; Feng, Z.; Karakalos, S.; Luo, L.; Qiao, Z.; Xie, X.; Wang, C.; Su, D.; Shao, Y.; Wu, G. Single Atomic Iron Catalysts for Oxygen Reduction in Acidic Media: Particle Size Control and Thermal Activation. *J. Am. Chem. Soc.* **2017**, *139*, 14143−14149.
(22) Jiao, L.; Wan, G.; Zhang, R.; Zhou, H.; Yu, S.-H.; Jiang, H.-L. From Metal-Organic Frameworks to Single-Atom Fe Implanted N-doped Porous Carbons: Efficient Oxygen Reduction in Both Alkaline and Acidic Media. *Angew. Chem., Int. Ed.* **2018**, *57*, 8525−8529.
(23) Meng, D.-L.; Chen, C.-H.; Yi, J.-D.; Wu, Q.; Liang, J.; Huang, Y.-B.; Cao, R. Migration-Prevention Strategy to Fabricate Single-Atom Fe Implanted N-Doped Porous Carbons for Efficient Oxygen Reduction. *Research* **2019**, *2019*, 12.
(24) Chen, X.; Bo, X.; Ren, W.; Chen, S.; Zhao, C. Microwave-assisted shock synthesis of diverse ultrathin graphene-derived materials. *Mater. Chem. Front.* **2019**, *3*, 1433−1439.
(25) Feng, D.; Gu, Z.-Y.; Li, J.-R.; Jiang, H.-L.; Wei, Z.; Zhou, H.-C. Zirconium-Metalloporphyrin PCN-222: Mesoporous Metal-Organic Frameworks with Ultrahigh Stability as Biomimetic Catalysts. *Angew. Chem., Int. Ed.* **2012**, *51*, 10307−10310.
(26) Nørskov, J. K.; Rossmeisl, J.; Logadottir, A.; Lindqvist, L.; Kitchin, J. R.; Bligaard, T.; Jonsson, H. Origin of the overpotential for oxygen reduction at a fuel-cell cathode. *J. Phys. Chem. B* **2004**, *108*, 17886−17892.
(27) Mano, N.; Soukharev, V.; Heller, A. A laccase-wiring redox hydrogel for efficient catalysis of O_2 electroreduction. *J. Phys. Chem. B* **2006**, *110*, 11180−11187.
(28) Blanford, C. F.; Heath, R. S.; Armstrong, F. A. A stable electrode for high-potential, electrocatalytic O2 reduction based on rational attachment of a blue copper oxidase to a graphite surface. *Chem. Commun.* **2007**, 1710−1712.
(29) Lu, X.; Du, L.; Wang, D.; Yang, P.; Liu, L.; Zhang, J.; An, M.; Levin, O.; Wang, J.; Ge, L. Highly Dispersed Cu−NX Moieties Embedded in Graphene: A Promising Electrocatalyst towards the Oxygen Reduction Reaction. *ChemElectroChem* **2018**, *5*, 3323−3329.
(30) Yu, H.; Fisher, A.; Cheng, D.; Cao, D. Cu,N-codoped Hierarchical Porous Carbons as Electrocatalysts for Oxygen Reduction Reaction. *ACS Appl. Mater. Interfaces* **2016**, *8*, 21431−21439.
(31) Lai, Q.; Zhu, J.; Zhao, Y.; Liang, Y.; He, J.; Chen, J. MOF-Based Metal-Doping-Induced Synthesis of Hierarchical Porous Cu-N/C Oxygen Reduction Electrocatalysts for Zn-Air Batteries. *Small* **2017**, *13*, 1700740.
(32) Cui, L.; Cui, L.; Li, Z.; Zhang, J.; Wang, H.; Lu, S.; Xiang, Y. A copper single-atom catalyst towards efficient and durable oxygen reduction for fuel cells. *J. Mater. Chem. A* **2019**, *7*, 16690−16695.
(33) Wu, H.; Li, H.; Zhao, X.; Liu, Q.; Wang, J.; Xiao, J.; Xie, S.; Si, R.; Yang, F.; Miao, S.; Guo, X.; Wang, G.; Bao, X. Highly doped and exposed Cu(I)-N active sites within graphene towards efficient oxygen reduction for zinc-air batteries. *Energy Environ. Sci.* **2016**, *9*, 3736−3745.
(34) Li, W.; Min, C.; Tan, F.; Li, Z.; Zhang, B.; Si, R.; Xu, M.; Liu, W.; Zhou, L.; Wei, Q.; Zhang, Y.; Yang, X. Bottom-Up Construction of Active Sites in a Cu-N4-C Catalyst for Highly Efficient Oxygen Reduction Reaction. *ACS Nano* **2019**, *13*, 3177−3187.
(35) Qu, Y.; Li, Z.; Chen, W.; Lin, Y.; Yuan, T.; Yang, Z.; Zhao, C.; Wang, J.; Zhao, C.; Wang, X.; Zhou, F.; Zhuang, Z.; Wu, Y.; Li, Y. Direct transformation of bulk copper into copper single sites via emitting and trapping of atoms. *Nat. Catal.* **2018**, *1*, 781−786.
(36) Chen, A.; Kong, A.; Fan, X.; Yang, X.; Li, C.; Chen, Z.; Shan, Y. High-efficiency copper-based electrocatalysts for oxygen electroreduction by heating metal-phthalocyanine at superhigh temperature. *Int. J. Hydrogen Energy* **2017**, *42*, 16557−16567.
(37) Reis, R. M.; Valim, R. B.; Rocha, R. S.; Lima, A. S.; Castro, P. S.; Bertotti, M.; Lanza, M. R. V. The use of copper and cobalt phthalocyanines as electrocatalysts for the oxygen reduction reaction in acid medium. *Electrochim. Acta* **2014**, *139*, 1−6.
(38) Jiang, Z.; Sun, W.; Shang, H.; Chen, W.; Sun, T.; Li, H.; Dong, J.; Zhou, J.; Li, Z.; Wang, Y.; Cao, R.; Sarangi, R.; Yang, Z.; Wang, D.; Zhang, J.; Li, Y. Atomic interface effect of a single atom copper catalyst for enhanced oxygen reduction reactions. *Energy Environ. Sci.* **2019**, *12*, 3508−3514.
(39) Sun, Y.; Silvioli, L.; Sahraie, N. R.; Ju, W.; Li, J.; Zitolo, A.; Li, S.; Bagger, A.; Arnarson, L.; Wang, X.; Moeller, T.; Bernsmeier, D.; Rossmeisl, J.; Jaouen, F.; Strasser, P. Activity-Selectivity Trends in the Electrochemical Production of Hydrogen Peroxide over Single-Site Metal-Nitrogen-Carbon Catalysts. *J. Am. Chem. Soc.* **2019**, *141*, 12372−12381.
(40) Zhang, Z.; Yang, S.; Dou, M.; Liu, H.; Gu, L.; Wang, F. Systematic study of transition-metal (Fe, Co, Ni, Cu) phthalocyanines as electrocatalysts for oxygen reduction and their evaluation by DFT. *RSC Adv.* **2016**, *6*, 67049−67056.

https://dx.doi.org/10.1021/acsaem.0c00704
ACS Appl. Energy Mater. XXXX, XXX, XXX−XXX

(41) Rao, K. J.; Vaidhyanathan, B.; Ganguli, M.; Ramakrishnan, P. A. Synthesis of inorganic solids using microwaves. *Chem. Mater.* **1999**, *11*, 882−895.
(42) Bilecka, I.; Niederberger, M. Microwave chemistry for inorganic nanomaterials synthesis. *Nanoscale* **2010**, *2*, 1358−1374.
(43) Khan, N. A.; Jhung, S. H. Synthesis of metal-organic frameworks (MOFs) with microwave or ultrasound: Rapid reaction, phase-selectivity, and size reduction. *Coord. Chem. Rev.* **2015**, *285*, 11−23.
(44) Kitchen, H. J.; Vallance, S. R.; Kennedy, J. L.; Tapia-Ruiz, N.; Carassiti, L.; Harrison, A.; Whittaker, A. G.; Drysdale, T. D.; Kingman, S. W.; Gregory, D. H. Modern Microwave Methods in Solid-State Inorganic Materials Chemistry: From Fundamentals to Manufacturing. *Chem. Rev.* **2014**, *114*, 1170−1206.
(45) Lin, Y.; Baggett, D. W.; Kim, J.-W.; Siochi, E. J.; Connell, J. W. Instantaneous Formation of Metal and Metal Oxide Nanoparticles on Carbon Nanotubes and Graphene via Solvent-Free Microwave Heating. *ACS Appl. Mater. Interfaces* **2011**, *3*, 1652−1664.
(46) Kang, S.; Choi, H.; Bin Lee, S.; Park, S. C.; Park, J. B.; Lee, S.; Kim, Y.; Hong, B. H. Efficient heat generation in large-area graphene films by electromagnetic wave absorption. *2D Materials* **2017**, *4*, 025037.
(47) Kim, K. H.; Cho, K. M.; Kim, D. W.; Kim, S. J.; Choi, J.; Bae, S. J.; Park, S.; Jung, H.-T. The Role of Layer-Controlled Graphene for Tunable Microwave Heating and Its Applications to the Synthesis of Inorganic Thin Films. *ACS Appl. Mater. Interfaces* **2016**, *8*, 5556−5562.
(48) Savaram, K.; Li, M.; Tajima, K.; Takai, K.; Hayashi, T.; Hall, G.; Garfunkel, E.; Osipov, V.; He, H. Dry microwave heating enables scalable fabrication of pristine holey graphene nanoplatelets and their catalysis in reductive hydrogen atom transfer reactions. *Carbon* **2018**, *139*, 861−871.
(49) Shadle, S. E.; Penner-Hahn, J. E.; Schugar, H. J.; Hedman, B.; Hodgson, K. O.; Solomon, E. I. X-ray absorption spectroscopic studies of the blue copper site: metal and ligand K-edge studies to probe the origin of the EPR hyperfine splitting in plastocyanin. *J. Am. Chem. Soc.* **1993**, *115*, 767−776.
(50) Kau, L. S.; Spira-Solomon, D. J.; Penner-Hahn, J. E.; Hodgson, K. O.; Solomon, E. I. X-ray absorption edge determination of the oxidation state and coordination number of copper. Application to the type 3 site in Rhus vernicifera laccase and its reaction with oxygen. *J. Am. Chem. Soc.* **1987**, *109*, 6433−6442.
(51) Savaram, K.; Li, M.; Tajima, K.; Takai, K.; Hayashi, T.; Hall, G.; Garfunkel, E.; Osipov, V.; He, H. Dry microwave heating enables scalable fabrication of pristine holey graphene nanoplatelets and their catalysis in reductive hydrogen atom transfer reactions. *Carbon* **2018**, *139*, 861−871.
(52) Qu, Y.; Li, Z.; Chen, W.; Lin, Y.; Yuan, T.; Yang, Z.; Zhao, C.; Wang, J.; Zhao, C.; Wang, X.; Zhou, F.; Zhuang, Z.; Wu, Y.; Li, Y. Direct transformation of bulk copper into copper single sites via emitting and trapping of atoms. *Nat. Catal.* **2018**, *1*, 781−786.
(53) Wu, J.-B.; Lin, M.-L.; Cong, X.; Liu, H.-N.; Tan, P.-H. Raman spectroscopy of graphene-based materials and its applications in related devices. *Chem. Soc. Rev.* **2018**, *47*, 1822−1873.
(54) Fei, H.; Dong, J.; Feng, Y.; Allen, C. S.; Wan, C.; Volosskiy, B.; Li, M.; Zhao, Z.; Wang, Y.; Sun, H.; An, P.; Chen, W.; Guo, Z.; Lee, C.; Chen, D.; Shakir, I.; Liu, M.; Hu, T.; Li, Y.; Kirkland, A. I.; Duan, X.; Huang, Y. General synthesis and definitive structural identification of MN4C4 single-atom catalysts with tunable electrocatalytic activities. *Nat. Catal.* **2018**, *1*, 63−72.
(55) Lu, X.; Du, L.; Wang, D.; Yang, P.; Liu, L.; Zhang, J.; An, M.; Levin, O.; Wang, J.; Ge, L. Highly Dispersed Cu−NX Moieties Embedded in Graphene: A Promising Electrocatalyst towards the Oxygen Reduction Reaction. *ChemElectroChem* **2018**, *5*, 3323−3329.
(56) Zhong, J.-H.; Zhang, J.; Jin, X.; Liu, J.-Y.; Li, Q.; Li, M.-H.; Cai, W.; Wu, D.-Y.; Zhan, D.; Ren, B. Quantitative correlation between defect density and heterogeneous electron transfer rate of single layer graphene. *J. Am. Chem. Soc.* **2014**, *136*, 16609−16617.
(57) Ramaswamy, N.; Mukerjee, S. Influence of Inner- and Outer-Sphere Electron Transfer Mechanisms during Electrocatalysis of Oxygen Reduction in Alkaline Media. *J. Phys. Chem. C* **2011**, *115*, 18015−18026.
(58) Ramaswamy, N.; Mukerjee, S. Fundamental Mechanistic Understanding of Electrocatalysis of Oxygen Reduction on Pt and Non-Pt Surfaces: Acid versus Alkaline Media. *Adv. Phys. Chem.* **2012**, *2012*, 17.
(59) Bard, A. J.; Faulkner, L. R. *Electrochemical Methods: Fundamentals and Applications*, 2nd ed.; John Wiley & Sons, Inc., 2000.
(60) Patel, M.; Feng, W.; Savaram, K.; Khoshi, M. R.; Huang, R.; Sun, J.; Rabie, E.; Flach, C.; Mendelsohn, R.; Garfunkel, E.; He, H. Microwave Enabled One-Pot, One-Step Fabrication and Nitrogen Doping of Holey Graphene Oxide for Catalytic Applications. *Small* **2015**, *11*, 3358−3368.
(61) Xu, J.; Lin, Y.; Connell, J. W.; Dai, L. Nitrogen-Doped Holey Graphene as an Anode for Lithium-Ion Batteries with High Volumetric Energy Density and Long Cycle Life. *Small* **2015**, *11*, 6179−6185.

https://dx.doi.org/10.1021/acsaem.0c00704
ACS Appl. Energy Mater. XXXX, XXX, XXX−XXX